SUPPORTING INFORMATION FOR:

Multi-Dimensional Mapping of Spin-Exchange Optical Pumping in Clinical-Scale Batch-Mode ^{129}Xe Hyperpolarizers

Panayiotis Nikolaou,[*,†] *Aaron M. Coffey,*[†,∞] *Kaili Ranta,*[‡] *Laura L. Walkup,*[§,•] *Brogan M. Gust,*[§] *Michael J. Barlow,*[//] *Matthew S. Rosen,*[⊥,#] *Boyd M. Goodson,*[§] *Eduard Y. Chekmenev*[*,†,∞,◇]

[†]Vanderbilt University Institute of Imaging Science (VUIIS), Department of Radiology, Nashville, Tennessee 37232, United States

[‡]Department of Physics, Southern Illinois University Carbondale, Illinois 62901, United States

[§]Department of Chemistry & Biochemistry, Southern Illinois University Carbondale, Illinois 62901, United States

[//] Sir Peter Mansfield Magnetic Resonance Centre, University of Nottingham, Nottingham, NG7 2RD, UK

[⊥]Massachusetts General Hospital/Athinoula A. Martinos Center for Biomedical Imaging, Boston, Massachusetts 02129, United States

[#]Department of Physics, Harvard University, Cambridge, Massachusetts 02138, United States

[∞]Department of Biomedical Engineering, [◇]Department of Biochemistry, Vanderbilt-Ingram Cancer Center, Nashville, Tennessee, 37205, Unites States

Experimental Methods

Volume Holographic Grating Laser Diode Array (VHG-LDA): The SEOP apparatus uses a 200 W LDA from QPC Lasers (P/N Brightlock Ultra-500 6507-Z002, Sylmar, California) that is frequency narrowed with "on-chip" volume holographic gratings (VHGs) that are integrated into the laser by having them written at the wafer level on the individual wafers of each diode through metal-organic chemical vapor deposition (MOCVD).[1] The VHG technology, which provides laser output that is spectrally narrowed to ~0.2–0.3 nm FWHM, an order-of-magnitude improvement compared to conventional broadband LDAs (FWHM~2–3 nm). The VHG-LDA also has a custom, integrated, single-piece, detachable optical assembly, which bolts directly onto the laser module. The optical assembly expands the emitted laser light to a single 2 in. diameter beam and converts the linear polarized light emitted from the laser into circular polarized light. Beam stops with heat sinks on either side of the polarizing beam-splitter (PBS) cube within the assembly dissipate the energy of unused portions of the laser output.

SEOP Oven was custom designed and 3D-printed from polycarbonate material to accommodate the SEOP process.[2] The oven was designed around the thermo-electric cooling (TEC) module (Kryotherm, Saint-Petersburg, Russia, P/N 380-24-AA), which provides variable temperature control for heating and cooling the SEOP-cell. The oven body and the SEOP-cell holders are printed as a single piece, thus ensuring that the SEOP-cell is always concentrically aligned with the laser and the oven's front anti-reflective (AR) coated optical window. Furthermore, a retro-reflection mirror is also incorporated into the oven, which reflects the transmitted laser light back through the longitudinal SEOP-cell axis, thus increasing the usable photon flux.

SEOP-cell: The cell is made from 2.125 in. outer diameter (OD), 2 in. inner diameter (ID) tubular Pyrex glass, 9.75 in. in length. The ends of this tubular glass are sealed using 2.125 in.

OD optical flats to create a 0.5 L inner volume. Two side stems are attached on the same side orthogonal to the main body, which are sealed with Teflon stopcocks that are used for loading the SEOP-cell with $^{129}Xe:N_2$ mixtures, and for transferring HP ^{129}Xe to a Tedlar bag or a phantom after the SEOP process is completed (the latter was used in the experiments described in this study). Each SEOP-cell used is pressure-tested to ~3.5 atm above atmospheric pressure.

Preparation of the SEOP-cells has been described earlier,[3-4] and will only be discussed briefly here. After pressure testing each SEOP-cell, it is then placed in a KOH/methanol base-bath for a 24 hour period to remove all impurities from the glass surface. The cell is then cleaned with distilled water and ultrasonically cleaned in a 50/50 water-methanol mix for ~1 hour before finally being rinsed and placed inside a low-temperature (~100 ºC) oven to remove the residual methanol. The dried cell's interior surface is then coated with siliconizing agent (SurfraSil, P/N PI-42800, Fisher Scientific) to increase the ^{129}Xe T_1 relaxation time. The coating solution is prepared by diluting 1 mL of SurfraSil in 9 mL of hexane. A portion of the resulting solution is pipetted into a clean SEOP-cell and swirled around for a few minutes to coat all glass surfaces. The solution is then removed and the cell is rinsed with hexane. The cell is then oven-dried once again, and it is then allowed to cool. The produced SEOP-cell is evacuated down to $< 10^{-3}$ Torr prior to placing it inside a glove box in preparation for loading it with ~250 mg of molten Rb metal under an inert (N_2) atmosphere.

Once the SEOP-cell is loaded with Rb, it is sealed (via its stopcocks) and removed from the glove box and placed on a gas manifold to be evacuated. Once evacuated, the cell is re-sealed and the Rb droplet is vaporized by heating it to distribute a fine layer of Rb coating throughout the cell. Because of outgassing of the Rb droplet, the Rb coating process may take a few cycles. When the coating is completed, the cell is then evacuated again, and loaded with the desired ^{129}Xe / N_2 gaseous mixture composition for use.

SEOP/*in situ* NMR Electromagnet: The homogeneous field used for SEOP and *in situ* NMR detection is generated from a four coil (**Fig. 1)** electro-magnet assembly (Acutran, Fombell, PA), which follow Barker electromagnet configuration described earlier.[2] The four individual coils of ~24 in. OD are connected in series and are operated with a single power supply (PSU) to generate a 4.00 mT (47 kHz ^{129}Xe Larmor frequency) or 1.10 mT (^{1}H Larmor frequency).

***In Situ* NMR Probe:** The surface RF coil was constructed using a ~0.5 in. ID former made of nylon material. The coil was made of ~400±40 turns with 30 gauge magnet wire (McMaster Carr) and resulted in ~1 in. OD. The RF coil windings were kept in place by two G10 plastic plates (~1.6 mm thick). The coil was tuned to 47 kHz using 3,700 pF capacitance by C22CF series capacitors (Dielectric Laboratories, Cazenovia, NY). The RF coil (which was not matched by capacitance) was connected directly to a Kea2 NMR spectrometer (Magritek, New Zealand) with high impedance RF probe interface and DC-1MHz duplexer configuration. The RF coil was placed immediately below the center of the SEOP-cell with an air gap of ~2±1 mm and mounted to the SEOP-oven body using ¼"-20 nylon rod.

NMR Spectroscopy and MRI at 47.5 mT*:* The *ex situ* NMR spectroscopy was carried out in the 47.5 mT 88 mm bore MRI system, which was in-house assembled using Magritek components (Wellington, New Zealand). Briefly, the system has 88 mm inner bore with 3 gradient (x, y, z) coils that allow for both gradient pulses and shimming. Dual channel X-^{1}H RF coil was employed, where X channel can be tuned to ^{13}C or ^{129}Xe frequencies of 508 kHz and 558.6 kHz respectively.[5-6] The X coil has 2 in. ID, and it is 8 in. long.[6] While ^{13}C RF pulses were calibrated as described previously, ^{129}Xe magnetization was large, potentially causing ADC overflow. To mitigate the potential signal-detection challenges and to be able to use gradient-echo (GRE) imaging sequences with small angle RF excitation pulses, a 20 μs (at ~80 mW) long RF pulse was employed for all ^{129}Xe detection. All spectra were acquired using 5 kHz spectral

width. 90° excitation RF pulse was used for detection of ^{13}C, while 2.7±0.1° RF pulse (20 μs at ~80 mW) was used for detection of hyperpolarized ^{129}Xe. 100 ms and 200 ms acquisition times were used for detection of ^{13}C and ^{129}Xe respectively. 256 averages were used for detection of the ^{13}C reference spectrum using a repetition time of 200 s (T_1 = 18 s at 47.5 mT), while all ^{129}Xe detection was carried out with a single scan.

Samples of hyperpolarized ^{129}Xe were collected in a 52 mL evacuated polypropylene sphere ("phantom") connected to the XeUS polarizer manifold via 1/8 in. OD, 1/16 in. ID PTFE tubing. The sample imaged in **Fig. 5** of the main document contained ~0.61 mmoles of ^{129}Xe spins using 26.44% natural abundance xenon and 50:50 mix of Xe:N_2 gas at 1000 Torr of Xe pressure and 1000 Torr N_2 pressure.

^{13}C reference sample contained 5.0 g of sodium 1-^{13}C-acetate dissolved in D_2O resulting in 22.4 mL total solution volume. The sample contained approximately 60 mmoles of ^{13}C spins.

Gradient-Echo (GRE) imaging of hyperpolarized ^{129}Xe: All images were acquired using a manufacturer-provided projection (2D) GRE imaging sequence. The following parameters were used: spectral width = 20 kHz, TE = 2.0 ms, TR ~ 80 ms (limited by the response time of the electronics) with 50% k-space sampling, 72x72 mm^2 FOV and 64x64 imaging matrix. The maximum voxel SNR was 48, **Fig. 5b** (main document).

Small-angle RF pulse-angle calibration using hyperpolarized ^{129}Xe and *ex situ* quantification of hyperpolarized ^{129}Xe was performed as follows: A 20 μs (at ~80 mW) long RF pulse was calibrated using direct detection of hyperpolarized ^{129}Xe. A series of GRE images was acquired, **Fig. 5** (main document). Every imaging acquisition was comprised of the 32 RF (64 projections with 50% k-space sampling) excitation pulses. The decay of hyperpolarized ^{129}Xe signal was monitored via signal intensities of the images, **Fig. 5** (main document). This decay allowed for measuring the effect of the RF pulse accounting for the T_1 losses. T_1 losses were measured using

separate spectroscopic measurements, e.g. **Fig. 4c** (main document), where only one RF pulse was applied every 1 minute, i.e. the ^{129}Xe polarization largely (>99%) depolarized via the T_1 relaxation mechanism. The application of trains of the RF pulses, **Fig. 5** (main document), as needed for imaging decreases residual polarization according to exponential decay. This exponential decay (corrected for T_1) yielded an effective total decay constant of ~162 s. The latter was used to compute the residual fractional magnetization at the time of 114 seconds as exp(-114/162) corresponding to 0.49 of the original magnetization. The latter was used to compute the RF excitation pulse angle (2.7°) as $\alpha = \arccos(0.49^{1/640})$, where 640 is the total number of RF pulses applied by the end of the image acquisitions, i.e. 114 seconds.

^{129}Xe polarization values were each calculated as the ratio of the signals and quantities of hyperpolarized and reference samples as well as the known polarization of the reference sample. It was additionally corrected for the small-angle RF excitation pulse, the small difference in their Larmor frequencies (between HP ^{129}Xe scan at 558.6 kHz and thermal ^{13}C scan at 508 kHz) and the magnetic moments as follows:

$$P(^{129}Xe) = P(^{13}C) \times \frac{\chi_{13C} \times S_{129Xe} \times (\gamma_{13C})^2}{\chi_{129Xe} \times S_{13C} \times (\gamma_{129Xe})^2 \times \sin\ \alpha}$$

where $P(^{13}C) = 4.1\times10^{-8}$ is the ^{13}C equilibrium polarization at 47.5 mT and 35 °C, χ_{13C} and χ_{129Xe} are quantities of ^{13}C and ^{129}Xe samples respectively, S_{13C} and S_{129Xe} are the NMR signal intensities of ^{13}C and ^{129}Xe samples respectively, and α is the small tipping angle of the excitation RF pulse used for detection of the hyperpolarized ^{129}Xe signal.

Appendix A: T_2* correction for polarization quantification using an external reference

In situ quantification of $\%P_{Xe}$ requires external standard for polarization calculation according to the following equation assuming the signals from reference and HP samples were acquired using the same RF excitation (in degrees) pulse:

$$\%P_{HP} = \frac{\%P_{REF} \times \chi_{REF} \times \gamma_{REF} \times S_{HP}}{\chi_{HP} \times \gamma_{HP} \times S_{REF}} \quad (1)$$

where $\%P_{REF}$ is % polarization of reference sample (e.g. water protons), S_{REF} and S_{HP} are signal of reference and hyperpolarized samples respectively, γ_{REF} and γ_{HP} are the gyromagnetic ratios of the reference and hyperpolarized spins respectively (e.g. protons and ^{129}Xe), and χ_{REF} and χ_{HP} are quantities or concentration of reference and hyperpolarized samples. The above equation holds true only in case if the entire Free Induction Decay (FID) signals from reference and hyperpolarized samples are recorded. However, in case if the signal is acquired using the RF circuit with significant 'dead' time or pre-acquisition delay using a pulse-and-acquire method, a significant fraction of NMR signal is lost during the initial FID evolution in the time domain. This might not be a limitation of quantification method described above as long as the FIDs of reference sample and HP sample are decaying with the same rate, i.e. T_2*(HP) ≈ T_2*(REF), corresponding to proportionately equal loss of NMR signal in both samples during pre-acquisition delay, T_{AQ}. This is not the case the 3D-printed polarizer used here, because T_{AQ} is appreciably large, and T_2*(HP) < T_2*(REF). As a result, a compensation factor C_{T2*} is introduced to accommodate for the losses of NMR signal due to T_2* and T_{AQ} as follows

$$\%P_{HP} = C_{T2*} \times \frac{\%P_{REF} \times \chi_{REF} \times \gamma_{REF} \times S_{HP}}{\chi_{HP} \times \gamma_{HP} \times S_{REF}} \quad (2)$$

T_2* values for water proton FID and HP ^{129}Xe FID was calculated by measuring the decay rate of FID and was T_2*(H_2O) = 15.5 ms and T_2*(^{129}Xe) = 10.4 ms. T_{AQ} was 4.0 ms.

The decay rate of FID is describes by exponential decay as

$$y = A \times \mathrm{e}^{-\frac{\mathrm{t}}{\mathrm{T2*}}} \tag{3}$$

The integral of the exponential function is used for calculation of the NMR signal intensity as

$$S = \int_{t1}^{t2} A \times \mathrm{e}^{-\frac{\mathrm{t}}{\mathrm{T2*}}} dt = -A \times T_2^* \times \mathrm{e}^{-\frac{\mathrm{t}}{\mathrm{T2*}}} \Big|_{t1}^{t2} \tag{4}$$

where t_1 and t_2 are NMR signal integration limits. It follows that full NMR signal with T_{AQ} = 0.0 ms is

$$S_{full} = -A \times T_2^* \times \mathrm{e}^{-\frac{\mathrm{t}}{\mathrm{T2*}}} \Big|_{0}^{\infty} = A \times T_2^* \times \left(\mathrm{e}^{-\frac{0}{\mathrm{T2*}}} - \mathrm{e}^{-\frac{\infty}{\mathrm{T2*}}}\right) = A \times T_2^* \tag{5}$$

The 'undetected' NMR signal during T_{AQ} is

$$S_{T_{AQ}} = -A \times T_2^* \times \mathrm{e}^{-\frac{\mathrm{t}}{\mathrm{T2*}}} \Big|_{0}^{T_{AQ}} = A \times T_2^* \times \left(\mathrm{e}^{-\frac{0}{\mathrm{T2*}}} - \mathrm{e}^{-\frac{T_{AQ}}{\mathrm{T2*}}}\right) = A \times T_2^* \times \left(1 - \mathrm{e}^{-\frac{T_{AQ}}{\mathrm{T2*}}}\right) \tag{6}$$

The observed NMR signal is therefore

$$S_{obs} = S_{full} - S_{T_{AQ}} = A \times T_2^* - A \times T_2^* \times \left(1 - \mathrm{e}^{-\frac{T_{AQ}}{\mathrm{T2*}}}\right) = A \times T_2^* \times \mathrm{e}^{-\frac{T_{AQ}}{\mathrm{T2*}}}, \tag{7}$$

and the percentage of observed signal with respect to the full signal is

$$\%S_{obs} = \frac{S_{obs}}{S_{full}} = \mathrm{e}^{-\frac{T_{AQ}}{\mathrm{T2*}}}, \tag{8}$$

$$\mathrm{C}_{T2*} = \frac{\%S_{obs(REF)}}{\%S_{obs(HP)}} = \frac{\mathrm{e}^{-\frac{T_{AQ}}{\mathrm{T2*(REF)}}}}{\mathrm{e}^{-\frac{T_{AQ}}{\mathrm{T2*(HP)}}}} = \mathrm{e}^{\frac{T_{AQ}}{\mathrm{T2*(HP)}} - \frac{T_{AQ}}{\mathrm{T2*(REF)}}} \tag{9}$$

For T_2*(H_2O) = 15.5 ms, T_2*(^{129}Xe) = 10.4 ms, and T_{AQ}, C_{T2*} is

$$\mathrm{C}_{T2*} = \mathrm{e}^{\frac{4.0}{10.4} - \frac{4.0}{15.5}} = 1.14 \tag{10}$$

Appendix B: Table S1. Summary Table of Studied SEOP Conditions

	Cell Temp (°C)	Laser Power (W)	Pmax (%)	Pmax Error (%)	Alt Pmax Error (%)	Tb (min)	Tb Error (min)	γ_{SEOP} (min^{-1})	γ_{SEOP} Error (min^{-1})
275+/-25 Torr Xe 1725 Torr N_2	62	100	66.1	2.27	6.01	88.9	5.00	0.011	6.33E-04
	72	100	76.5	0.55	6.96	46.3	0.80	0.022	3.73E-04
	82	100	84.1	0.36	7.64	24.8	0.40	0.040	6.50E-04
	92	100	82.6	1.00	7.51	13.3	0.90	0.075	5.09E-03
	92	125	87.5	0.55	7.95	9.9	0.40	0.101	4.08E-03
	92	142	88.3	1.45	8.02	9.5	0.90	0.105	9.97E-03
	62	170	66.5	2.45	6.05	58.9	4.10	0.017	1.18E-03
	72	170	83.1	0.73	7.55	26.5	0.80	0.038	1.14E-03
	82	170	95.3	1.00	8.66	13.2	0.60	0.076	3.44E-03
	Cell Temp (°C)	**Laser Power (W)**	**Pmax (%)**	**Pmax Error (%)**	**Alt Pmax Error (%)**	**Tb (min)**	**Tb Error (min)**	**γ_{SEOP} (min^{-1})**	**γ_{SEOP} error (min^{-1})**
515+/-25 Torr Xe 1485 Torr N_2	52	100	40.5	0.30	1.97	94.6	1.30	0.011	1.45E-04
	62	100	51.1	0.30	2.48	64.6	0.80	0.015	1.92E-04
	72	100	61.7	0.20	2.99	29.3	0.30	0.034	3.49E-04
	80	100	62.7	0.20	3.04	14.8	0.20	0.068	9.13E-04
	72	125	67.9	0.20	3.29	26.4	0.30	0.038	4.30E-04
	80	125	68.1	0.50	3.30	14.3	0.50	0.070	2.45E-03
	72	142	69.3	0.50	3.37	22.7	0.70	0.044	1.36E-03
	80	142	70.6	0.20	3.43	13.6	0.20	0.074	1.08E-03
	77	170	73.4	0.90	3.56	14	0.90	0.071	4.59E-03
	Cell Temp (°C)	**Laser Power (W)**	**Pmax (%)**	**Pmax Error (%)**	**Alt Pmax Error (%)**	**Tb (min)**	**Tb Error (min)**	**γ_{SEOP} (min^{-1})**	**γ_{SEOP} error (min^{-1})**
1000+/-25 Torr Xe 1000 Torr N_2	42	100	13.2	0.10	0.33	84.7	1.80	0.012	2.51E-04
	52	100	25.3	0.10	0.63	81.5	1.00	0.012	1.51E-04
	62	100	45.7	0.90	1.14	95	3.10	0.011	3.43E-04
	72	100	48.9	0.13	1.22	40	0.36	0.025	2.25E-04
	80	100	45.7	0.10	1.14	20	0.20	0.050	5.00E-04
	62	142	51.1	0.40	1.28	49.7	0.70	0.020	2.83E-04
	72	142	55.7	0.20	1.39	23.5	0.20	0.043	3.62E-04
	52	170	44.1	0.70	1.10	41.5	1.50	0.024	8.71E-04
	65	170	59.5	0.60	1.49	36.3	1.00	0.028	7.59E-04
	Cell Temp (°C)	**Laser Power (W)**	**Pmax (%)**	**Pmax Error (%)**	**Alt Pmax Error (%)**	**Tb (min)**	**Tb Error (min)**	**γ_{SEOP} (min^{-1})**	**γ_{SEOP} error (min^{-1})**
1500+/-25 Torr Xe 500 Torr N_2	52	100	16.7	0.20	0.28	108.5	3.02	0.009	2.57E-04
	62	100	20.7	0.23	0.34	61.8	2.20	0.016	5.76E-04
	72	100	29.6	0.39	0.49	57.1	2.19	0.018	6.70E-04
	82	100	26.7	0.27	0.44	20.5	1.06	0.049	2.52E-03
	92	100	15.7	0.36	0.26	7.6	1.32	0.132	2.30E-02
	62	125	34.9	0.42	0.58	58.6	2.25	0.017	6.56E-04
	72	125	35.2	0.36	0.59	30.4	1.21	0.033	1.31E-03
	82	125	19.1	0.20	0.32	10.5	0.92	0.096	8.39E-03
	62	142	38.1	0.31	0.64	42.8	1.13	0.023	6.18E-04
	72	142	33.2	0.24	0.55	20.8	0.91	0.048	2.11E-03
	52	170	39.6	0.32	0.66	51.7	1.49	0.019	5.56E-04
	62	170	41.3	0.37	0.69	29.7	1.15	0.034	1.30E-03
	Cell Temp (°C)	**Laser Power (W)**	**Pmax (%)**	**Pmax Error (%)**	**Alt Pmax Error (%)**	**Tb (min)**	**Tb Error (min)**	**γ_{SEOP} (min^{-1})**	**γ_{SEOP} error (min^{-1})**
2000+/-25 Torr Xe 200 Torr N_2	52	100	8.9	0.06	0.11	37.7	0.90	0.027	6.35E-04
	62	100	21.2	0.13	0.27	42.0	0.85	0.024	4.81E-04
	72	100	28.9	0.08	0.36	24.9	0.28	0.040	4.58E-04
	82	100	19.0	0.05	0.24	12.0	0.15	0.083	1.06E-03
	52	125	10.2	0.09	0.13	35.8	1.02	0.028	7.92E-04
	62	125	29.0	0.08	0.36	42.7	0.45	0.023	2.45E-04
	72	125	30.5	0.08	0.38	22.0	0.25	0.045	5.25E-04
	52	142	17.1	0.06	0.21	57.5	0.74	0.017	2.24E-04
	62	142	26.9	0.07	0.34	40.1	0.45	0.025	2.81E-04
	72	142	30.4	0.25	0.38	17.1	0.67	0.058	2.28E-03
	52	170	19.2	0.10	0.24	54.0	0.92	0.019	3.15E-04
	62	170	31.4	0.10	0.39	36.4	0.44	0.027	3.31E-04

Table S1 summarizes all SEOP results collected under variable laser power, temperature, and xenon density; where: *Cell Temp* refers to the temperature measured at the surface of the SEOP-cell; *Laser Power* is the measured laser output power at the exit of the 2 in. diameter optical assembly module; $\%P_{max}$ is the maximum ^{129}Xe percent polarization at steady-state optical pumping obtained as the extrapolated value of the curve fitting to the model of mono-exponential growth; $\%P_{max}$ *error* is the error calculated for the same SEOP-cell for a series of experiments using the same Xe density; and *Alt* $\%P_{max}$ *error* is the $\%P_{max}$ error associated when comparing results to a different series of Xe densities. This alternative error takes into account the uncertainty related to the Xe and N_2 gas filling, i. e. ± 25 Torr; *Tb* is the $\%P_{Xe}$ build-up time constant obtained directly from the fitting model of mono-exponential growth; *Tb error* is the error of the exponential fit used to fit the build-up curve; γ_{SEOP} is the SEOP rate constant obtained from the exponential fit of the build-up curve, which is a sum of the spin exchange rate and the xenon spin destruction rate, see the main text; γ_{SEOP} *error* is the calculated error of the spin exchange optical pumping rate. These results were used to produce the 2D contour plots of **Fig. 3** in the main text using Microcal Origin software.

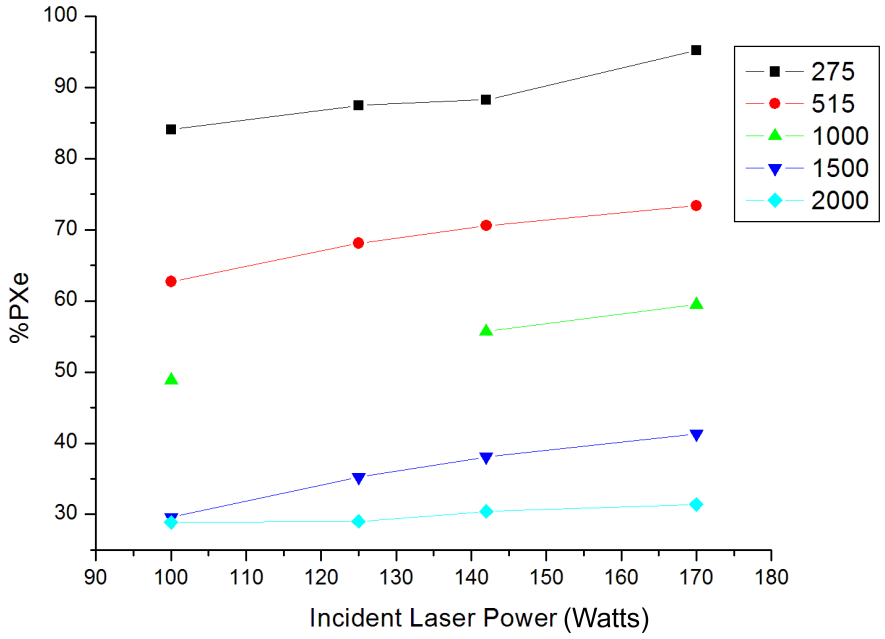

Figure S1. Data taken from Table 1 showing that in general, ^{129}Xe polarization is still growing with increasing laser power up through the maximum available incident laser power (~170 W). The Legend indicates the curves corresponding to cells containing 275, 515, 1000, 1500, and 2000 Torr Xe partial pressure.

References

1. Whiting, N.; Nikolaou, P.; Eschmann, N. A.; Barlow, M. J.; Lammert, R.; Ungar, J.; Hu, W.; Vaissie, L.; Goodson, B. M. Using Frequency-Narrowed, Tunable Laser Diode Arrays with Integrated Volume Holographic Gratings for Spin-Exchange Optical Pumping at High Resonant Fluxes and Xenon Densities. *Appl. Phys. B-Lasers Opt.* **2012,** *106* (4), 775-788.
2. Nikolaou, P.; Coffey, A. M.; Walkup, L. L.; Gust, B.; LaPierre, C.; Koehnemann, E.; Barlow, M. J.; Rosen, M. S.; Goodson, B. M.; Chekmenev, E. Y. A 3D-Printed High Power Nuclear Spin Polarizer. *J. Am. Chem. Soc.* **2014,** *136* (4), 1636–1642.
3. Nikolaou, P.; Coffey, A. M.; Walkup, L. L.; Gust, B. M.; Whiting, N.; Newton, H.; Barcus, S.; Muradyan, I.; Dabaghyan, M.; Moroz, G. D.; Rosen, M.; Patz, S.; Barlow, M. J.; Chekmenev, E. Y.; Goodson, B. M. Near-Unity Nuclear Polarization with an 'Open-Source' ^{129}Xe Hyperpolarizer for NMR and MRI. *Proc. Natl. Acad. Sci. U. S. A.* **2013,** *110* (35), 14150-14155.
4. Nikolaou, P.; Coffey, A. M.; Walkup, L. L.; Gust, B. M.; Whiting, N. R.; Newton, H.; Muradyan, I.; Dabaghyan, M.; Ranta, K.; Moroz, G.; Patz, S.; Rosen, M. S.; Barlow, M. J.; Chekmenev, E. Y.; Goodson, B. M. Xena: An Automated 'Open-Source' ^{129}Xe Hyperpolarizer for Clinical Use. *Magn. Reson. Imaging* **2014**, *32*, 541-550.
5. Waddell, K. W.; Coffey, A. M.; Chekmenev, E. Y. In Situ Detection of Phip at 48 Mt: Demonstration Using a Centrally Controlled Polarizer. *J. Am. Chem. Soc.* **2011,** *133* (1), 97-101.
6. Coffey, A. M.; Shchepin, R. V.; Wilkens, K.; Waddell, K. W.; Chekmenev, E. Y. A Large Volume Double Channel ^{1}H-X RF Probe for Hyperpolarized Magnetic Resonance at 0.0475 Tesla. *J. Magn. Reson.* **2012,** *220*, 94–101.